ARTICLES

A dual-Ca^{2+}-sensor model for neurotransmitter release in a central synapse

Jianyuan Sun[1,2], Zhiping P. Pang[1], Dengkui Qin[1], Abigail T. Fahim[4], Roberto Adachi[4] & Thomas C. Südhof[1,2,3]

Ca^{2+}-triggered synchronous neurotransmitter release is well described, but asynchronous release—in fact, its very existence—remains enigmatic. Here we report a quantitative description of asynchronous neurotransmitter release in calyx-of-Held synapses. We show that deletion of synaptotagmin 2 (*Syt2*) in mice selectively abolishes synchronous release, allowing us to study pure asynchronous release in isolation. Using photolysis experiments of caged Ca^{2+}, we demonstrate that asynchronous release displays a Ca^{2+} cooperativity of ~2 with a Ca^{2+} affinity of ~44 μM, in contrast to synchronous release, which exhibits a Ca^{2+} cooperativity of ~5 with a Ca^{2+} affinity of ~38 μM. Our results reveal that release triggered in wild-type synapses at low Ca^{2+} concentrations is physiologically asynchronous, and that asynchronous release completely empties the readily releasable pool of vesicles during sustained elevations of Ca^{2+}. We propose a dual-Ca^{2+}-sensor model of release that quantitatively describes the contributions of synchronous and asynchronous release under conditions of different presynaptic Ca^{2+} dynamics.

Two modes of Ca^{2+}-triggered neurotransmitter release have been described: fast synchronous release predominates in all synapses during low-frequency action-potential firing[1,2]; slower asynchronous release mediates synaptic transmission in some synapses during high-frequency action-potential trains[3–7], but remains a minor component in other synapses[1,2]. Precise measurements of Ca^{2+} triggering of synchronous release were obtained in the calyx-of-Held synapse, which allows simultaneous patching of pre- and postsynaptic neurons, and enables monitoring of Ca^{2+} currents and capacitance of nerve terminals[8–12]. Such measurements revealed that the Ca^{2+} sensor for synchronous release exhibits an apparent cooperativity of ~5, and an apparent K_d of ~10 or ~105 μM Ca^{2+} (refs 11 and 12). In vertebrate synapses, synaptotagmin 1, 2 and 9 (Syt1, Syt2 and Syt9) function as Ca^{2+} sensors for fast synchronous release[13–18], exhibit a binding stoichiometry of 5 Ca^{2+} ions per molecule, and a micromolar Ca^{2+} affinity (note that 12 other synaptotagmins are expressed in the brain that do not function as Ca^{2+} sensors for fast release). Of Syt1, Syt2 and Syt9, Syt2 is a likely Ca^{2+} sensor for synchronous release at the calyx synapse because a mutation that decreases Syt2 levels impairs synchronous release from calyx terminals[19].

In synapses with predominantly asynchronous release during high-frequency action-potential trains, asynchronous release outcompetes synchronous release during the action-potential train[3–7]. Measurements of asynchronous release suggested a higher apparent Ca^{2+} affinity, but the same Ca^{2+} cooperativity as synchronous release[20,21]. These properties would explain the ability of asynchronous release to out-compete synchronous release during high-frequency action-potential trains, because the accumulating residual Ca^{2+} in the train would trigger asynchronous release in the intervals between action potentials at Ca^{2+} levels at which synchronous release cannot be induced. Consistent with this notion, Ca^{2+} chelators such as EGTA block asynchronous release during high-frequency action-potential trains but have less effect on synchronous release[3–6,22]. According to this view, synapses without predominantly asynchronous release during high-frequency trains, such as the calyx synapse, either lack asynchronous release, or have efficient Ca^{2+} buffering and Ca^{2+} extrusion mechanisms that prevent accumulation of residual Ca^{2+} (refs 23 and 24). Moreover, the similar apparent Ca^{2+} cooperativity of synchronous and asynchronous release suggested that asynchronous release could be a modification of synchronous release[25], indicating that there are no separate universal synchronous and asynchronous release pathways[24]. Indeed, quantitative models of release that are based on the assumption of a single Ca^{2+} sensor are widely applicable[11,12]. These models, however, are inaccurate at low Ca^{2+} concentrations; even a recently refined model that proposes allosterically modulated release machinery with a single Ca^{2+} sensor is unable to accurately predict release rates at low Ca^{2+} concentrations[25]. Thus, at present, no accurate quantitative model for neurotransmitter release is available. Evaluating asynchronous release and generating an accurate quantitative model for release is difficult because asynchronous release has primarily been characterized in synapses that have a strong synchronous component, which could have contaminated the measurements[20,21], and because the biophysical properties of asynchronous release remain unknown. However, these questions have wide implications for our understanding of synaptic transmission because an accurate description of asynchronous release is required for any quantitative model of synaptic transmission. We now provide such a description in the calyx-of-Held synapse, and demonstrate that asynchronous release represents a separate and distinct release pathway that is likely to be universally present in synapses.

Syt2 knockout blocks synchronous release

Mice lacking Syt2 initially develop normally, but perish after postnatal day 21 (P21). In the calyx-of-Held synapse, we detected no coexpression of Syt1 with Syt2 at any time between P5 and P14, or of Syt9 at P11 (Fig. 1a, and Supplementary Fig. 2). Moreover, we observed no compensatory increases of Syt1 in Syt2-deficient calyces, and found no overall change in protein composition (Fig. 1b, and Supplementary Figs 2–4). Thus, calyx terminals express only one (Syt2) of the three synaptotagmins (Syt1, Syt2 and Syt9) that serve as Ca^{2+} sensors for synchronous release[18,19], presumably because Syt2

[1]Departments of Neuroscience and [2]Molecular Genetics, and [3]Howard Hughes Medical Institute, The University of Texas Southwestern Medical Center, Dallas, Texas 75390, USA. [4]Department of Pulmonary Medicine, The University of Texas M.D. Anderson Cancer Center, Houston, Texas 77030, USA.

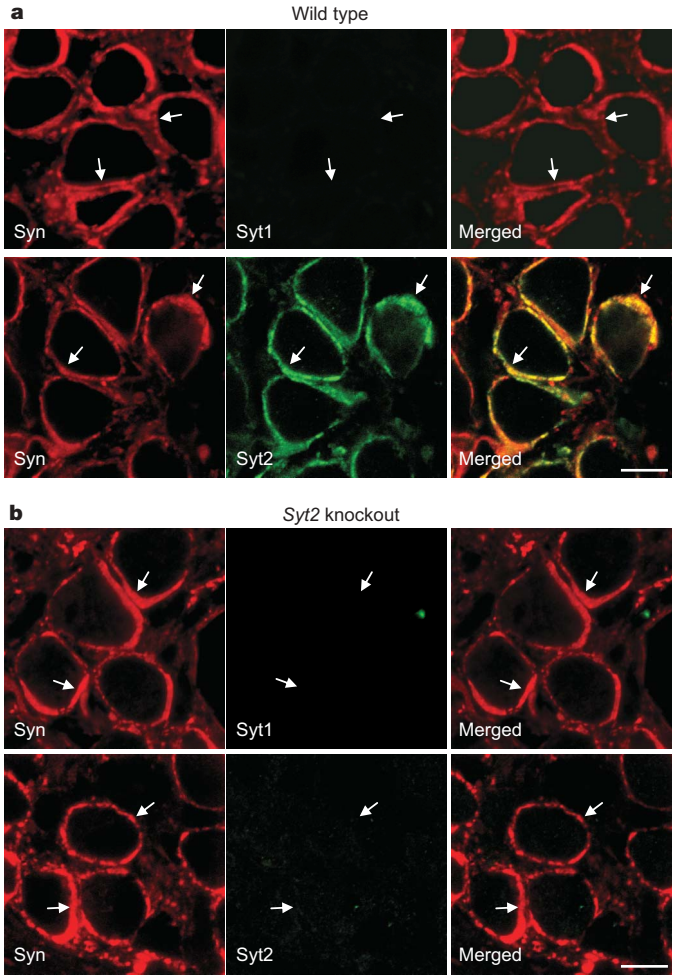

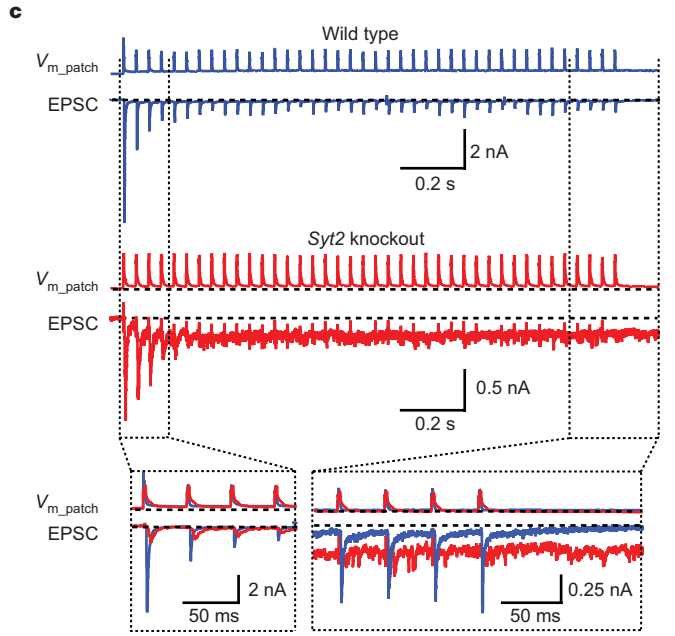

Figure 1 | Calyx synapses in Syt2-deficient mice. **a**, **b**, Immunofluorescence analysis of brainstem sections from wild-type (**a**) and Syt2-deficient mice (**b**) at P11 with antibodies to synapsins 1–3 (Syn; red; left panels) and Syt1 or Syt2 (green; middle panels; Supplementary Fig. 2). Merged images are shown on the right with coincident staining in yellow (scale bar, 10 μm, applies to all panels; arrows, synapses). **c**, EPSCs recorded in response to 25 Hz action-potential stimulation induced by a cell-attached presynaptic pipette (V_{m_patch}, extracellular voltage in the patched area). The inset at the bottom shows a superposition of wild-type and mutant traces.

is the fastest Ca^{2+} sensor[18] and the calyx synapse is specialized for precise fast responses[8,9].

To determine the effect of the Syt2 deletion on release, we examined brainstem slices from 7–9-day-old mice. Using cell-attached patches on presynaptic calyx terminals, we induced a train of presynaptic action potentials and measured postsynaptic responses by whole-cell recordings. Strikingly, evoked synaptic responses in Syt2-deficient terminals were small and delayed, with release being increasingly triggered in the inter-stimulus intervals during the stimulus train (Fig. 1c). These responses are consistent with the

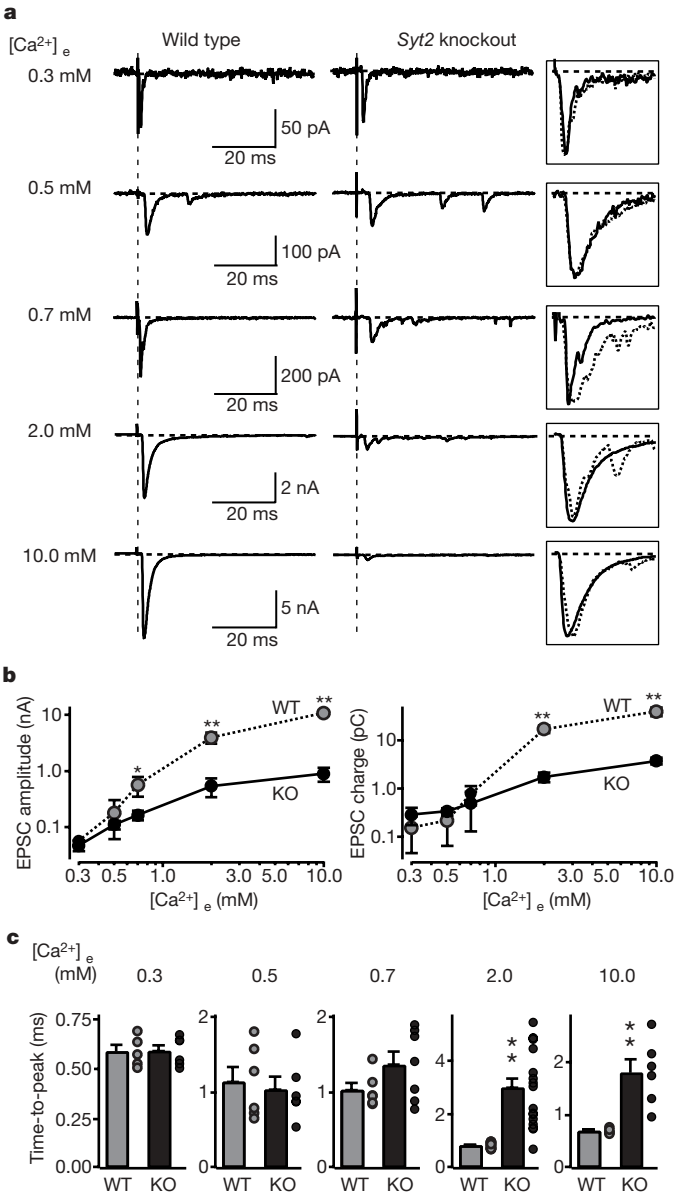

Figure 2 | Synaptic transmission evoked by isolated action potentials. Postsynaptic voltage-clamp recordings of ESPCs evoked by afferent fibre stimulation in wild-type (left) and Syt2-deficient calyx synapses (right) at the indicated $[Ca^{2+}]_e$ in the presence of 50 μM AP-5. **a**, Representative EPSCs. Boxed traces on right display scaled superimposed EPSCs to illustrate EPSC kinetics. **b**, Double-logarithmic plots of EPSC amplitudes (left panel) or EPSC charge transfer (right panel) as a function of $[Ca^{2+}]_e$ (mean ± s.e.m.; number of recordings/$[Ca^{2+}]_e$: wild-type (WT), 5/0.3 mM, 6/0.5 mM, 6/0.7 mM, 14/2 mM, 5/10 mM; KO, 6/0.3 mM, 6/0.5 mM, 7/0.7 mM, 17/2 mM, 6/10 mM). **c**, Summary graphs of the rise times of EPSCs recorded for the indicated $[Ca^{2+}]_e$. For each Ca^{2+} concentration, the bar depicts mean ± s.e.m.; dots next to the bar exhibit individual data points (*, $P < 0.05$; **, $P < 0.01$; Student's *t*-test).

notion that, in the absence of Syt2 as the Ca^{2+} sensor for synchronous release, accumulating Ca^{2+} during the stimulus train triggers asynchronous release.

To characterize this asynchronous release, we induced presynaptic action potentials by afferent fibre stimulations, and recorded excitatory postsynaptic currents (EPSCs) at different extracellular Ca^{2+} concentrations ($[Ca^{2+}]_e = 0.3–10$ mM). At 0.3–0.7 mM $[Ca^{2+}]_e$, wild-type and mutant terminals exhibited similar amounts of release (Fig. 2a, b). At 2 mM and 10 mM $[Ca^{2+}]_e$, however, Syt2-deficient terminals displayed >10-fold smaller EPSC amplitudes and charge transfers than wild-type terminals (Fig. 2a, b). Moreover, at 2 mM $[Ca^{2+}]_e$ (a nearly physiological concentration), Syt2-deficient synapses were ~3-times slower in reaching the EPSC maximum (Fig. 2c), and exhibited ~5-fold slower release kinetics (measured as the time to achieve 50% synaptic charge transfer; wild-type (WT) = 4.9 ± 0.7 ms; *Syt2* knockout (KO) = 26.8 ± 1.7 ms (means ± s.e.m.); $P < 0.01$; Supplementary Fig. 5). We conclude that deletion of Syt2 severely impairs fast synchronous release in the calyx-of-Held synapse, but leaves a slower, asynchronous form of Ca^{2+}-triggered release intact. In addition, the deletion of Syt2, like that of Syt1 in forebrain[19], increased the frequency of miniature spontaneous release events but did not alter the size and kinetics of these events (Supplementary Fig. 6).

A potential concern is that, because the *Syt2* knockout mice die at P21–P24, the knockout neurons may not be healthy. However, at P7–P14, when we analyse the *Syt2* knockout mice, the knockout mice are not visibly distressed, the protein composition of their brainstems is not detectably altered (Supplementary Fig. 4), and the basic electrical properties of the postsynaptic calyx neurons are not impaired (Supplementary Table 1). Thus, the changes we observe in the knockout mice are probably specifically caused by the deletion of Syt2.

Ca^{2+} currents and readily releasable pool size

In presynaptic terminals of the calyx of Held, action potentials gate Ca^{2+} influx via P/Q- and N-type Ca^{2+} channels[26,27]. Because Syt1 interacts with Ca^{2+} channels[28–30], we tested whether deletion of the highly homologous Syt2 impairs Ca^{2+} channel function. We simultaneously patched presynaptic calyx terminals and postsynaptic neurons in the presence of drugs that block action-potential propagation, AMPA(α-amino-3-hydroxy-5-methylisoxazole-propionic acid)-receptor desensitization, and NMDA (*N*-methyl-D-aspartic acid)-receptor activation. We then recorded presynaptic Ca^{2+} currents and postsynaptic EPSCs in response to prolonged depolarization (4 ms predepolarization from −80 to +80 mV followed by 50 ms depolarization to +20 mV)[31]. Deletion of Syt2 caused no detectable change in the amplitudes of presynaptic Ca^{2+} currents, electrical charge transfer mediated by the Ca^{2+} channels (integrated over 100 ms), or the *I*/*V* relationship, suggesting that Syt2 is not involved in regulating Ca^{2+} channels (Figs 3a–3c, and Supplementary Figs 7 and 8).

The 50 ms depolarization in Fig. 3a depletes the readily releasable pool (RRP) of vesicles by inducing a prolonged increase in intracellular $[Ca^{2+}]_i$ (ref. 31). Postsynaptic recordings of synaptic responses showed that deletion of Syt2 depressed the peak amplitude of the depolarization-induced EPSC ~2-fold, slowed its rise time ~3-fold, and increased its latency ~5-fold (Fig. 3d–f). However, the Syt2 deletion did not alter the total synaptic charge transfer induced by the 50 ms presynaptic depolarization (Fig. 3g; integrated over 2 s). Thus, deletion of Syt2 did not affect the size of the RRP, and asynchronous release induces exocytosis of the entire RRP of vesicles in the absence of Syt2, albeit with a slower time course.

To compare the size of the RRP in wild-type and *Syt2* knockout mice by an independent approach, we puffed a 2 M sucrose solution onto the terminal for 1 s, and integrated the synaptic charge transfer of the induced EPSCs over 2 s (Figs 3h, i, and Supplementary Fig. 9). Again, no difference between wild-type and Syt2-deficient terminals was detected. The absolute size of the RRP determined after sustained depolarization was larger than the RRP size measured by puffing of hypertonic sucrose (Fig. 3). This difference may be due to the distinct measurement conditions used (ESPCs induced by depolarization but not by sucrose were monitored in the presence of cyclothiazide as a blocker of receptor desensitization); in addition, Ca^{2+}-dependent mobilization of the RRP during the depolarization may have increased its size during the monitoring period[32].

Ca^{2+} dependence of release

To characterize the Ca^{2+} dependence of transmitter release at wild-type and Syt2-deficient synapses, we determined the peak release rates in calyx terminals as a function of the presynaptic intracellular Ca^{2+} concentration $[Ca^{2+}]_i$. For Ca^{2+} concentrations of <1 μM, we employed two methods: (1) injection of terminals via the patch pipette with defined concentrations of Ca^{2+} and Ca^{2+} buffers, or (2) with caged Ca^{2+} (9 mM DM-nitrophen, 8.6 mM $CaCl_2$, and various Ca^{2+} buffers) that is released by flash photolysis with a weak laser pulse (Supplementary Fig. 10)[11,12,33,34]. For Ca^{2+} concentrations of >1 μM, we employed only the flash photolysis method with a

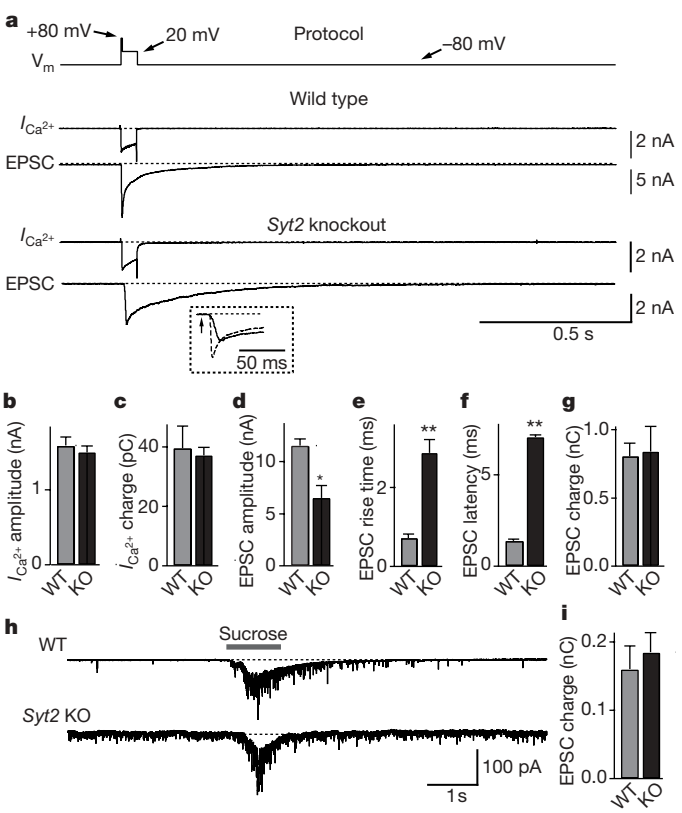

Figure 3 | RRP size, Ca^{2+} currents and release kinetics in Syt2-deficient calyx synapses. a, Experimental protocol involving a 4-ms predepolarization followed by a 50-ms depolarization (upper line), and representative traces of presynaptic Ca^{2+} currents ($I_{Ca^{2+}}$) and postsynaptic EPSCs (lower traces). The inset displays an expansion of the initial phase of the EPSCs from wild-type (dotted line) and Syt2-deficient terminals (continuous line; arrow = start of Ca^{2+} current). Experiments were performed by simultaneous pre- and postsynaptic voltage-clamp recordings in calyx terminals at P7–P9 in 0.1 μM tetrodotoxin, 0.1 mM cyclothiazide, 1 mM kynurenic acid and 50 μM D-AP5. **b**–**g**, Quantifications of Ca^{2+} current amplitudes (**b**), Ca^{2+}-current electrical charge transfer (**c**, integrated over 100 ms), EPSC amplitudes (**d**), EPSC rise times (**e**; 20–80%), EPSC latencies (**f**; from onset of Ca^{2+} current to 10% of the EPSC) and EPSC charge transfer (**g**; integrated over 2 s) induced by sustained presynaptic depolarization. Data shown are mean ± s.e.m. (WT, $n = 12$; KO, $n = 14$). **h**, **i**, Representative traces (**h**) and summary graphs (**i**; integrated over 5 s) of the electric charge transfer of synaptic responses induced by 1-s applications of 2 M sucrose via a glass pipette positioned ~5 μm from the calyx (mean ± s.e.m.; WT, $n = 10$; KO, $n = 11$).

stronger laser pulse. Flash photolysis of caged Ca^{2+} produces a rapid and spatially uniform, defined rise in $[Ca^{2+}]_i$, which we monitored *in situ* in the terminals, using co-injected Ca^{2+}-indicator dyes. To cover the entire range of Ca^{2+} concentrations examined (0.1–15 μM), we employed three different Ca^{2+}-indicator dyes (Fura-2, Fura-4F and Fura-6F), and calibrated the Ca^{2+} signals directly in the calyx terminals (Supplementary Fig. 10). Finally, we quantified vesicle exocytosis by deconvolution of evoked EPSCs, using a measured miniature EPSC waveform to calculate the release rates[31] (see Methods and Supplementary Materials).

We first elevated $[Ca^{2+}]_i$ to concentrations of 0.05–1.0 μM. Increases of $[Ca^{2+}]_i$ to <0.2 μM induced an enhancement in miniature EPSC frequency but no clearcut evoked EPSCs (Fig. 4a). At these Ca^{2+} concentrations, release was slightly higher in Syt2-deficient than wild-type synapses (Fig. 4e), presumably because deletion of Syt2 increases the resting frequency of miniature EPSCs (Supplementary Fig. 6). At $[Ca^{2+}]_i$ of 0.2–1.0 μM, wild-type and Syt2-deficient synapses exhibited indistinguishable release rates, independent of whether the $[Ca^{2+}]_i$ was constantly clamped with Ca^{2+} buffers, or acutely raised by photolysis of caged Ca^{2+} with a weak flash (Fig. 4, and Supplementary Fig. 11). Thus, as observed for action-potential-induced release at low $[Ca^{2+}]_e$ (Fig. 2), deletion of Syt2 does not impair release evoked at low $[Ca^{2+}]_i$. This result suggests that, even in wild-type synapses, release at low $[Ca^{2+}]_i$ is physiologically mediated by the asynchronous Ca^{2+} sensor, a conclusion that is consistent with previously described properties of release induced by low $[Ca^{2+}]_i$ (ref. 35).

We next examined larger increases in $[Ca^{2+}]_i$ produced by flash photolysis of caged Ca^{2+}. In wild-type neurons, a peak release rate of ~24 vesicles ms^{-1} was evoked when $[Ca^{2+}]_i$ was elevated to 2 μM (Fig. 4c). The peak release rate steeply increased to ~1,750 vesicles ms^{-1} when $[Ca^{2+}]_i$ was raised to 9.2 μM, demonstrating a very high Ca^{2+} cooperativity (Fig. 4d). In Syt2-deficient synapses, conversely, a 2 μM $[Ca^{2+}]_i$ rise caused release with a peak rate of 3.7 vesicle ms^{-1}. Elevation of $[Ca^{2+}]_i$ to 10.5 μM only increased the release rate to 31 vesicles ms^{-1}, revealing a ~50-fold lower release rate and a much lower Ca^{2+} cooperativity in Syt2-deficient synapses than in wild-type synapses.

Figure 4e displays the Ca^{2+} dependence of the peak release rate obtained from 78 wild-type (open symbols) and 106 Syt2-deficient terminals (filled symbols), plotted on logarithmic coordinates (see Supplementary Table 2 for numerical values). Whereas at $[Ca^{2+}]_i$ of <1 μM, the vesicular release rates are not decreased in Syt2-deficient terminals, at $[Ca^{2+}]_i > 2$ μM, deletion of Syt2 reduced the peak transmitter release rate 10–50-fold compared to wild-type synapses. In the most dynamic range of 0.7–5.0 μM $[Ca^{2+}]_i$, the relation of the peak release rate to $[Ca^{2+}]_i$ follows a fifth power function in wild-type terminals, but only a second power function in Syt2-deficient terminals (Fig. 4e). At higher $[Ca^{2+}]_i$, release saturates in wild-type synapses, but not in knockout synapses. Thus, whereas release triggered at $[Ca^{2+}]_i = 0.2$–1.0 μM exhibits a similarly low Ca^{2+} cooperativity and magnitude in wild-type and Syt2-deficient synapses, release triggered at $[Ca^{2+}]_i > 1$ μM exhibits a dramatically different Ca^{2+} cooperativity and magnitude in wild-type and mutant synapses.

A potential concern with a genetic study is that a compensatory developmental change could lead to the expression of a non-physiological Ca^{2+} sensor in mutant synapses. However, release at low $[Ca^{2+}]_i$, measured with $[Ca^{2+}]_i$ raised by two different methods, is indistinguishable between wild-type and Syt2-deficient synapses. This fact argues strongly against such a developmental change in the mutant terminals because such a change should have affected the behaviour of Ca^{2+}-triggered release at all Ca^{2+} concentrations. Moreover, the good prediction of release in both wild-type and mutant synapses by our quantitative model described below is inconsistent with such a change.

A dual-Ca^{2+}-sensor model of release

Previous Ca^{2+} photolysis studies on calyx synapses prompted formulation of a quantitative model of neurotransmitter release with a single Ca^{2+} sensor for release (referred to here as the 'conventional

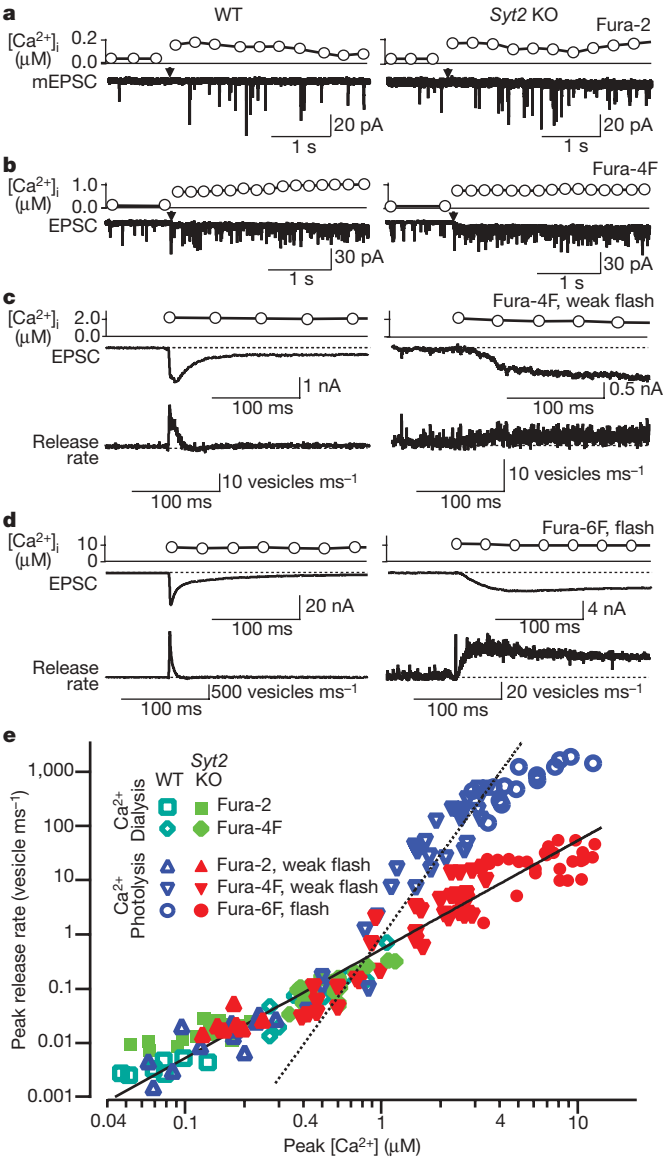

Figure 4 | Relationship between peak vesicular release rates and $[Ca^{2+}]_i$ in calyx terminals. EPSCs were recorded in calyx synapses in the double-patch configuration at P7–P9 in the presence of 50 μM D-AP5 in all experiments, and of 0.1 mM cyclothiazide in experiments in which release rates were quantified by deconvolution (for example, panels **c** and **d**), and of 2 mM γ-DGG in experiments in which $[Ca^{2+}]_i$ was raised to >3 μM (for example, panel **d**). Presynaptic $[Ca^{2+}]_i$ increases were achieved by photolysis of caged Ca^{2+} dialysed into the terminal, or by dialysis of buffered Ca^{2+} at low $[Ca^{2+}]$. $[Ca^{2+}]_i$ was monitored optically using three different Ca^{2+}-sensitive dyes as indicated (for *in situ* calibration of $[Ca^{2+}]_i$, see Supplementary Materials). **a**–**d**, Representative experiments in wild-type (left panels) and Syt2-deficient calyces (right panels) at four characteristic Ca^{2+} concentrations; the Ca^{2+}-indicator dyes used are shown on the right. Panels **c** and **d** also display the vesicle release rate as calculated by EPSC deconvolutions. **e**, Summary graph of peak release rates and $[Ca^{2+}]_i$ ($n = 78$ for wild-type (open symbols), 106 for Syt2-deficient terminals (filled symbols); green symbols represent the data obtained by dialysis of Ca^{2+} buffers into the terminals via the patch pipette). The dashed line represents a fit of a fifth power function to the data from wild-type terminals at $[Ca^{2+}]_i = >1$μM ($y = 0.90x^5$); the solid line represents the fit of a second power function to the data from mutant terminals ($y = 0.54x^2$); note that the solid line also fits the wild-type responses at low $[Ca^{2+}]_i$.

one-sensor model')[11,12]. These models, however, were unable to predict release at low $[Ca^{2+}]_i$ (Fig. 5a), presumably because this release—as depicted in Figs 2 and 4—is primarily carried by the asynchronous Ca^{2+} sensor. Partly to remedy this problem, and partly to account for the change in release induced by phorbol esters, an allosteric model of release was proposed[25] that improves prediction of the Ca^{2+} dependence of peak release rates (Fig. 5a). The allosteric model, however, also postulates a single Ca^{2+} sensor, and underestimates the time-to-peak rate at lower $[Ca^{2+}]_i$ (Fig. 5b). To formulate a more accurate model, we developed a dual-Ca^{2+}-sensor kinetic model that is based on the current information (Fig. 5c). This model postulates that (1) synchronous release is triggered by Ca^{2+} binding to a Ca^{2+} sensor with a Ca^{2+} cooperativity of ~5, consistent with the Ca^{2+}-binding properties of synaptotagmins; (2) asynchronous release is triggered by Ca^{2+} binding to an unidentified Ca^{2+} sensor with a Ca^{2+} cooperativity of ~2 (Fig. 4); and (3) spontaneous release occurs with an effectivity factor C to account for the change in spontaneous release in synaptotagmin-deficient synapses[17,19] (Supplementary Fig. 6). The dual-Ca^{2+}-sensor model assumes that these three release pathways compete with each other, and operate on the same vesicle pools.

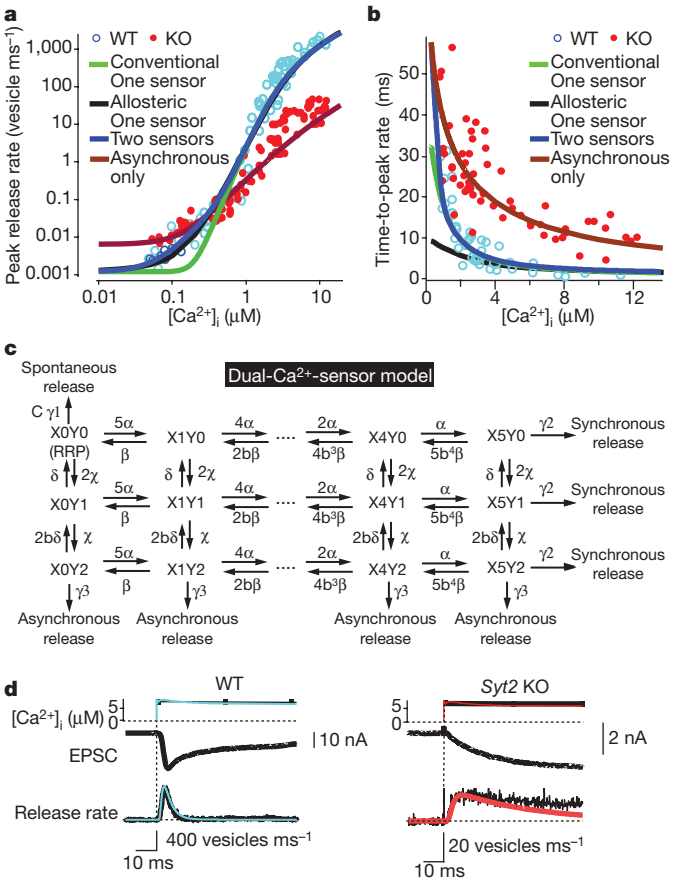

Figure 5 | A dual-Ca^{2+}-sensor model for neurotransmitter release. a, b, Fits of the Ca^{2+}-photolysis data from wild-type and Syt2-deficient calyces for the peak release rate (**a**) and time-to-peak rate (**b**) to the conventional 1-sensor model[11,12], the allosteric 1-sensor model[25], the 2-sensor model, and the 2-sensor model with inactivation of the synchronous Ca^{2+} sensor (see Supplementary Materials and Supplementary Figs 10–13 for details; RRP is set to 3,000 vesicles[11,12]). **c**, Reaction scheme. γ1, γ2, γ3, rates of spontaneous, synchronous and asynchronous release, respectively (defined as the fraction of the RRP released per second); α and β, and χ and δ = k_{on} and k_{off} for Ca^{2+} action for synchronous and asynchronous release, respectively; X0–X5 and Y0–Y2, Ca^{2+}-binding states of the Ca^{2+} sensor for synchronous (X) and asynchronous release (Y), respectively (note that X0Y0 = RRP); b, cooperativity factor[11,12,34]. The curve-fitting parameters were (only γ1 differs between wild-type and knockout): $\alpha = 1.53 \times 10^8\ M^{-1}s^{-1}$, $\beta = 5{,}800\ s^{-1}$, b = 0.25; $\chi = 2.94 \times 10^6\ M^{-1}s^{-1}$, $\delta = 130\ s^{-1}$, $\gamma 1 = 0.417 \times 10^{-3}\ s^{-1}$ in wild type and $2.23 \times 10^{-3}\ s^{-1}$ in knockout; $\gamma 2 = 6{,}000\ s^{-1}$; $\gamma 3 = 6{,}000\ s^{-1}$. γ1 was measured experimentally, b and γ2 were from ref. 11, and γ3 was assumed to be equal to γ2 on the basis of the postulate that Ca^{2+} binding to the asynchronous and synchronous release Ca^{2+} sensors will trigger the same release rates because both empty the entire RRP. **d**, Local $[Ca^{2+}]_i$ signal predicted by the Ca^{2+}-relaxation model (Supplementary Fig. 12) and transmitter release rates predicted by the dual-Ca^{2+}-sensor model in wild-type (left) and *Syt2*-knockout calyces (right). Uppermost panels, measured and predicted $[Ca^{2+}]_i$ (black, and blue or red, respectively); middle panels, recorded EPSCs; lowest panels, vesicular release rates deconvoluted from EPSCs (black), and predicted by the model (blue or red).

Our parameters for synchronous release are squarely in the middle between the two previous estimates in calyx synapses[11,12], but our parameters for asynchronous release differ from previous suggestions[20,21], probably because previous suggestions were based on extrapolations of asynchronous release in the continued presence of synchronous release, which may have contaminated the estimates. Although the dual-Ca^{2+}-sensor model thus reveals that asynchronous release exhibits a relatively low apparent Ca^{2+} affinity and release rate, the model still predicts that asynchronous release is the major physiological mode of synaptic transmission at low $[Ca^{2+}]_i$ because its lower degree of Ca^{2+} cooperativity renders asynchronous release more effective at low $[Ca^{2+}]_i$. At high $[Ca^{2+}]_i$, conversely, synchronous release dominates because the predicted k_{on} for synchronous release is ~100-fold higher than that for asynchronous release (Fig. 5).

Summary

Here we show that among synaptotagmin isoforms that act as Ca^{2+} sensors for synchronous release[18], calyx terminals only express Syt2 (Fig. 1, and Supplementary Fig. 2). We demonstrate that in calyx terminals, Syt2 is essential for Ca^{2+} triggering of fast synchronous release (Fig. 2), but not for Ca^{2+} influx or vesicle priming (Fig. 3). Thus, Syt2—as suggested for Syt1 in forebrain synapses[13]—is selectively required for Ca^{2+} triggering of fast release in calyx-of-Held synapses. We show that although asynchronous release contributes little to action-potential-induced vesicle exocytosis in wild-type calyx synapses at physiological $[Ca^{2+}]_i$, asynchronous release triggers exocytosis of the entire RRP on prolonged increases in $[Ca^{2+}]_i$ in *Syt2*-knockout calyx synapses (Fig. 3). Therefore, synchronous and asynchronous release act on the same vesicle pools. Moreover, release at low $[Ca^{2+}]_i$ exhibits a similar magnitude and Ca^{2+} dependence in wild-type and Syt2-deficient synapses, suggesting that release at low $[Ca^{2+}]_i$ is normally asynchronous, and that asynchronous release does not change in the knockout mice.

Traditionally, asynchronous release is explained by three competing hypotheses: (1) asynchronous and synchronous release share the same Ca^{2+} sensor, but differ in the coupling of vesicles to Ca^{2+} channels, the state of the vesicles, and/or the Ca^{2+}-buffering mechanisms involved[24,25,36,37]; (2) synchronous and asynchronous release are mediated by the same Ca^{2+} sensor but use different, allosterically regulated vesicle pools[38]; or (3) different Ca^{2+} sensors with distinct properties mediate synchronous and asynchronous release[13]. Clearly the distance between synaptic vesicles and Ca^{2+} channels is a major determinant of the vesicular release probability, and

differences in the Ca^{2+} channel proximity of vesicles probably contribute to the vesicles' heterogeneity of release probabilities[39]. Moreover, undoubtedly, different pools of vesicles exist and contribute to the heterogeneity of release probabilities at a synapse. Nevertheless, these differences are probably unrelated to the differences between synchronous and asynchronous release, but are rather involved in regulating all release. Indeed, the following findings suggest that synchronous and asynchronous release are caused by independent mechanisms.

- Synchronous and asynchronous release exhibit qualitatively different properties, as shown by the unexpectedly low Ca^{2+} affinity and distinctly low Ca^{2+} cooperativity of asynchronous release, and by its persistence after synchronous release was selectively eliminated on deletion of Syt2 (Fig. 4).
- Asynchronous release is independent of the proximity of synaptic vesicles to Ca^{2+} channels, because our flash photolysis experiments produce a uniform increase in $[Ca^{2+}]_i$ that bypasses Ca^{2+}-channel activation (Fig. 4).
- Single-Ca^{2+}-sensor models[11,12] adequately describe release at higher $[Ca^{2+}]_i$ but are unable to account for release at low $[Ca^{2+}]_i$. Even the sophisticated allosteric model[25] underestimates the time-to-peak release rate at low $[Ca^{2+}]_i$ (Fig. 5b).
- Release in wild-type and Syt2-deficient terminals is identical at low $[Ca^{2+}]_i$ (Figs 2 and 4), suggesting that this type of release is physiologically asynchronous. Moreover, asynchronous release becomes apparent during high-frequency action-potential trains in wild-type calyx synapses (Supplementary Fig. 14), consistent with studies of the precise kinetics of individual EPSCs demonstrating that asynchronous release in the calyx normally occurs even during isolated action protentials[40].

The definition of the biophysical properties of asynchronous, Ca^{2+}-triggered release made it possible to formulate a quantitative model for neurotransmitter release that probably applies to all synapses (Fig. 5). Our model indicates that the Ca^{2+} sensors for synchronous and asynchronous release operate in competition with each other, with the asynchronous Ca^{2+} sensor being slower but able to bind Ca^{2+} at lower concentrations, whereas the synchronous Ca^{2+} sensor is faster with a higher Ca^{2+} cooperativity. As a result, in this competition, the synchronous Ca^{2+} sensor 'wins' during pulses of high Ca^{2+} concentrations, whereas the asynchronous Ca^{2+} sensor prevails during sustained phases of lower Ca^{2+} concentrations (Fig. 5). Within this framework, differences between synapses are primarily determined by which synaptotagmin isoform is being used as the Ca^{2+} sensor for synchronous release[18], and by the accumulation of residual Ca^{2+} in the intervals between action potentials during stimulus trains (that is, by the Ca^{2+}-buffering properties of a nerve terminal)[34–36,41]. It is of interest here that, fittingly, the calyx terminals with their exquisitely fast-release properties use as the synchronous Ca^{2+} sensor only Syt2, the fastest of the three Ca^{2+} sensors[18].

METHODS SUMMARY

Syt2-knockout mice were bred and genotyped as described[17]. Brain slices (200 μm) containing MNTB were prepared in a parasagital orientation from P7–P9 mice (for double-patch or presynaptic cell-attached recording), or in a transverse orientation from P10–P14 mice (for fibre stimulation and purely postsynaptic recordings), and employed for single and/or double whole-cell recordings of nerve terminals and MNTB neurons with presynaptic electrical stimulation or stimulation by Ca^{2+} uncaging or Ca^{2+} dialysis, largely as described[11,12,31,38,42]. Ca^{2+} uncaging was achieved with an intense ultraviolet radiation pulse from a frequency-tripled YAG-ND laser, and the resulting Ca^{2+} concentrations were measured *in situ* by ratiometric fluorescence imaging of nerve terminals filled with Fura-2, Fura-4F, or Fura-6F (Supplementary Fig. 10)[34,43]. Ca^{2+} dyes were calibrated *in situ*. Release rates were calculated using the Neher deconvolution program (http://www.mpibpc.mpg.de/groups/neher/software/index.html) with a miniature EPSC size of 30 pA and a measured waveform[31]. We applied the different kinetic models to fit the data in our experiments (Fig. 5a, b, and Supplementary Figs 11 and 13), with the conventional and allosteric single-Ca^{2+}-sensor kinetic models simulated as described[11,12,25] (Supplementary Fig. 13). In our dual-Ca^{2+}-sensor model, each vesicle in the RRP can be released via three independent pathways (Fig. 5): (1) Ca^{2+}-independent fusion in the spontaneous mode, that is, direct exocytosis of vesicles from the RRP with a release rate of $\gamma 1$. An effectivity factor (C) to account for the change in spontaneous release rate in Syt1- and Syt2-deficient synapses was included; (2) synchronous Ca^{2+}-evoked fusion mode triggered by full occupancy of the five binding sites of the synchronous release Ca^{2+} sensor[12,25]; or (3) asynchronous Ca^{2+}-evoked release triggered by occupancy of two Ca^{2+}-binding sites of an unidentified Ca^{2+} sensor.

Full Methods and any associated references are available in the online version of the paper at www.nature.com/nature.

Received 20 August; accepted 24 September 2007.

1. Meinrenken, C. J., Borst, J. G. & Sakmann, B. Local routes revisited: the space and time dependence of the Ca^{2+} signal for phasic transmitter release at the rat calyx of Held. *J. Physiol. (Lond.)* **547,** 665–689 (2003).
2. Schneggenburger, R. & Neher, E. Presynaptic calcium and control of vesicle fusion. *Curr. Opin. Neurobiol.* **15,** 266–274 (2005).
3. Atluri, P. P. & Regehr, W. G. Delayed release of neurotransmitter from cerebellar granule cells. *J. Neurosci.* **18,** 8214–8227 (1998).
4. Lu, T. & Trussell, L. O. Inhibitory transmission mediated by asynchronous transmitter release. *Neuron* **26,** 683–694 (2000).
5. Hagler, D. J. Jr & Goda, Y. Properties of synchronous and asynchronous release during pulse train depression in cultured hippocampal neurons. *J. Neurophysiol.* **85,** 2324–2334 (2001).
6. Otsu, Y. *et al.* Competition between phasic and asynchronous release for recovered synaptic vesicles at developing hippocampal autaptic synapses. *J. Neurosci.* **24,** 420–433 (2004).
7. Hefft, S. & Jonas, P. Asynchronous GABA release generates long-lasting inhibition at a hippocampal interneuron–principal neuron synapse. *Nature Neurosci.* **8,** 1319–1328 (2005).
8. Forsythe, I. D. Direct patch recording from identified presynaptic terminals mediating glutamatergic EPSCs in the rat CNS, *in vitro*. *J. Physiol. (Lond.)* **479,** 381–387 (1994).
9. Borst, J. G. & Sakmann, B. Calcium influx and transmitter release in a fast CNS synapse. *Nature* **383,** 431–434 (1996).
10. Sun, J. Y. & Wu, L. G. Fast kinetics of exocytosis revealed by simultaneous measurements of presynaptic capacitance and postsynaptic currents at a central synapse. *Neuron* **30,** 171–182 (2001).
11. Schneggenburger, R. & Neher, E. Intracellular calcium dependence of transmitter release rates at a fast central synapse. *Nature* **406,** 889–893 (2000).
12. Bollmann, J. H., Sakmann, B. & Borst, J. G. Calcium sensitivity of glutamate release in a calyx-type terminal. *Science* **289,** 953–957 (2000).
13. Geppert, M. *et al.* Synaptotagmin I: a major Ca^{2+} sensor for transmitter release at a central synapse. *Cell* **79,** 717–727 (1994).
14. Fernandez-Chacon, R. *et al.* Synaptotagmin I functions as a Ca^{2+}-regulator of release probability. *Nature* **410,** 41–49 (2001).
15. Stevens, C. F. & Sullivan, J. M. The synaptotagmin C_2A domain is part of the calcium sensor controlling fast synaptic transmission. *Neuron* **39,** 299–308 (2003).
16. Nagy, G. *et al.* Different effects on fast exocytosis induced by synaptotagmin 1 and 2 isoforms and abundance, but not by phosphorylation. *J. Neurosci.* **26,** 632–643 (2006).
17. Pang, Z. P. *et al.* Synaptotagmin-2 is essential for survival and contributes to Ca^{2+} triggering of neurotransmitter release in central and neuromuscular synapses. *J. Neurosci.* **26,** 13493–13504 (2006).
18. Xu, J., Mashimo, T. & Südhof, T. C. Synaptotagmin-1, -2, and -9: Ca^{2+}-sensors for fast release that specify distinct presynaptic properties in subsets of neurons. *Neuron* **54,** 801–812 (2007).
19. Pang, Z. P., Sun, J., Rizo, J., Maximov, A. & Südhof, T. C. Genetic analysis of Syt2 in spontaneous and Ca^{2+}-triggered neurotransmitter release. *EMBO J.* **25,** 2039–2050 (2006).
20. Goda, Y. & Stevens, C. F. Two components of transmitter release at a central synapse. *Proc. Natl Acad. Sci. USA* **91,** 12942–12946 (1994).
21. Ravin, R., Spira, M. E., Parnas, H. & Parnas, I. Simultaneous measurement of intracellular Ca^{2+} and asynchronous transmitter release from the same crayfish bouton. *J. Physiol. (Lond.)* **501,** 251–262 (1997).
22. Maximov, A. & Südhof, T. C. Autonomous function of synaptotagmin 1 in triggering asynchronous release independent of asynchronous release. *Neuron* **48,** 547–554 (2005).
23. Chuhma, N. & Ohmori, H. Role of Ca^{2+} in the synchronization of transmitter release at calyceal synapses in the auditory system of rat. *J. Neurophysiol.* **87,** 222–228 (2002).
24. Schneggenburger, R. & Forsythe, I. D. The calyx of Held. *Cell Tissue Res.* **326,** 311–337 (2006).
25. Lou, X., Scheuss, V. & Schneggenburger, R. Allosteric modulation of the presynaptic Ca^{2+} sensor for vesicle fusion. *Nature* **435,** 497–501 (2005).
26. Iwasaki, S. & Takahashi, T. Developmental changes in calcium channel types mediating synaptic transmission in rat auditory brainstem. *J. Physiol. (Lond.)* **509,** 419–423 (1998).

27. Wu, L. G., Westenbroek, R. E., Borst, J. G., Catterall, W. A. & Sakmann, B. Calcium channel types with distinct presynaptic localization couple differentially to transmitter release in single calyx-type synapses. *J. Neurosci.* **19,** 726–736 (1999).
28. Leveque, C. *et al.* Purification of the N-type calcium channel associated with syntaxin and synaptotagmin. A complex implicated in synaptic vesicle exocytosis. *J. Biol. Chem.* **269,** 6306–6312 (1994).
29. Charvin, N. *et al.* Direct interaction of the calcium sensor protein synaptotagmin I with a cytoplasmic domain of the α1A subunit of the P/Q-type calcium channel. *EMBO J.* **16,** 4591–4596 (1997).
30. Zhong, H., Yokoyama, C. T., Scheuer, T. & Catterall, W. A. Reciprocal regulation of P/Q-type Ca^{2+} channels by SNAP-25, syntaxin and synaptotagmin. *Nature Neurosci.* **2,** 939–941 (1999).
31. Sakaba, T. & Neher, E. Quantitative relationship between transmitter release and calcium current at the calyx of Held synapse. *J. Neurosci.* **21,** 462–476 (2001).
32. Stevens, C. F. & Wesseling, J. F. Activity-dependent modulation of the rate at which synaptic vesicles become available to undergo exocytosis. *Neuron* **21,** 415–424 (1998).
33. Mulkey, R. M. & Zucker, R. S. Action potentials must admit calcium to evoke transmitter release. *Nature* **350,** 153–155 (1991).
34. Heidelberger, R., Heinemann, C., Neher, E. & Matthews, G. Calcium dependence of the rate of exocytosis in a synaptic terminal. *Nature* **371,** 513–515 (1994).
35. Awatramani, G. B., Price, G. D. & Trussell, L. O. Modulation of transmitter release by presynaptic resting potential and background calcium levels. *Neuron* **48,** 109–121 (2005).
36. Taschenberger, H., Scheuss, V. & Neher, E. Release kinetics, quantal parameters and their modulation during short-term depression at a developing synapse in the rat CNS. *J. Physiol. (Lond.)* **568,** 513–537 (2005).
37. Wadel, K., Neher, E. & Sakaba, T. The coupling between synaptic vesicles and Ca^{2+} channels determines fast neurontransmitter release. *Neuron* **53,** 563–575 (2007).
38. Wölfel, M., Lou, X. & Schneggenburger, R. A mechanism intrinsic to the vesicle fusion machinery determines fast and slow transmitter release at a large CAN synapse. *J. Neurosci.* **27,** 3198–3210 (2007).
39. Trommershauser, J., Schneggenburger, R., Zippelius, A. & Neher, E. Heterogeneous presynaptic release probabilities: functional relevance for short-term plasticity. *Biophys. J.* **84,** 1563–1579 (2003).
40. Kushmerick, C., Renden, R. & von Gersdorff, H. Physiological temperatures reduce the rate of vesicle pool depletion and short-term depression via an acceleration of vesicle recruitment. *J. Neurosci.* **26,** 1366–1377 (2006).
41. Bollmann, J. H. & Sakmann, B. Control of synaptic strength and timing by the release-site Ca^{2+} signal. *Nature Neurosci.* **8,** 426–434 (2005).
42. Sun, J., Bronk, P., Liu, X., Han, W. & Südhof, T. C. Synapsins regulate use-dependent synaptic plasticity in the calyx of Held by a Ca^{2+}/calmodulin-dependent pathway. *Proc. Natl Acad. Sci. USA* **103,** 2880–2885 (2006).
43. Grynkiewicz, G., Poenie, M. & Tsien, R. Y. A new generation of Ca^{2+} indicators with greatly improved fluorescence properties. *J. Biol. Chem.* **260,** 3440–3450 (1985).

Supplementary Information is linked to the online version of the paper at www.nature.com/nature.

Acknowledgements We thank I. Kornblum, A. Roth, L. Fan and J. Mitchell for excellent technical assistance, and J. Bollmann, X. Lou and R. Schneggenburger for advice. This study was supported by a grant from NARSAD (to J.S.) and by The University of Texas M. D. Anderson Cancer Center Physician Scientist Program (R.A.).

Author Contributions J.S. performed the electrophysiology and photolysis experiments and modelling. Z.P.P. carried out the biochemical, immunohistochemical, and mouse genetics experiments; D.Q. participated in the electrophysiology and photolysis experiments; A.T. F. and R.A. generated the *Syt2* knockout mice, and T.C.S. and J.S. designed the experiments and wrote the manuscript.

Author Information Reprints and permissions information is available at www.nature.com/reprints. Correspondence and requests for materials should be addressed to J.S. (Jianyuan.Sun@UTSouthwestern.edu) or T.C.S. (Thomas.Sudhof@UTSouthwestern.edu).

METHODS

***Syt2*-knockout mice.** Syt2-deficient mice were bred and genotyped as described[17] (see Supplementary Materials for detailed methods). All analyses were performed on littermate offspring from heterozygous matings ('wild-type mice' refers to those that are homo- or heterozygous for the wild-type allele).

Slice electrophysiology. All experiments involved postsynaptic whole-cell recordings with an Axopatch 200B amplifier (Axon Instruments). Presynaptic whole-cell recordings were obtained with an EPC-9 amplifier (HEKA). The pre- and postsynaptic series resistances (<15 MΩ and 7 MΩ) were compensated by 60% and 98% (lag 10 μs), respectively. Both pre- and postsynaptic currents were low-pass-filtered at 5 kHz and digitized at 20 kHz. Six recording configurations were employed (see Supplementary Materials for details): (1) Presynaptic cell-attached current injections to induce presynaptic action-potential trains with postsynaptic whole-cell recordings that monitor the evoked EPSCs (Fig. 1c). Stimulations were applied as 40 presynaptic current injections of 1 nA for 3 ms at 50 Hz. (2) Presynaptic afferent fibre stimulations with postsynaptic whole-cell voltage-clamp recordings (Fig. 2). Stimuli were applied with a bipolar electrode delivering 3–30 V for 0.1 ms. (3) Double-patch recordings by simultaneous pre- and postsynaptic whole-cell voltage-clamp recordings to measure the presynaptic RRP and Ca^{2+} currents (Figs 3a–g). Stimulations consist of a presynaptic 4 ms predepolarization to 70–80 mV, followed by 50 ms depolarization to 20 mV. (4) Sucrose stimulation with postsynaptic whole-cell voltage-clamp recordings to measure the RRP (Fig. 3h, i). Stimulation involves puffing 2 M sucrose in bath solution onto the target terminal with a pipette that is located about 5 μm from the calyx. (5) Double-patch experiments for simultaneous measurements of presynaptic $[Ca^{2+}]_i$ and postsynaptic ESPCs with manipulation of the presynaptic $[Ca^{2+}]_i$ (Fig. 4). Stimulations were effected either by dialysis of Ca^{2+}-containing solutions into the terminal via the presynaptic pipette (Fig. 4e, and Supplementary Fig. 11a, b), or by flash photolysis of DM-nitrophen/Ca^{2+} (Fig. 4, and Supplementary Fig. 11c). Release rate was estimated by deconvolution[31]. (6) Mini recordings (Supplementary Fig. 6 and Supplementary Methods).

All recordings were performed in the presence of 50 μM D-AP5 in the bath; in addition, for the double-patch experiments in (3) and (4), we added 0.1 mM cyclothiazide and 1 mM kynurenic acid or 2 mM γ-DGG when strong flash photolysis was given, resulting in $[Ca^{2+}]_i$ of >3 μM, in which case the obtained EPSCs were multiplied by 2 because control experiments determined that 2 mM γ-DGG decreased the EPSC amplitude twofold.

Ca^{2+} uncaging and Ca^{2+} imaging. The Ca^{2+}-uncaging and Ca^{2+}-imaging setup (Supplementary Fig. 5a) used an intense ultraviolet radiation pulse from a frequency-tripled YAG-ND laser (355 nm, Surelite I, Continuum) for Ca^{2+} uncaging. Ca^{2+} concentrations were measured *in situ* by ratiometric fluorescence imaging of nerve terminals filled with Fura-2, Fura-4F or Fura-6F (refs 34, 43). Ca^{2+}-indicator dyes were excited with an ultraviolet light source at 340 nm and 380 nm (energy ≤175 W) using a monochromator (DG-4, Sutter Instrument). The laser pulse was coupled into the epifluorescence port of an Axioskop and combined with the ultraviolet light using a beam-splitter (customized 90%T/10%R for 355 nm with a bandwith of <10 nm, Chroma Tech). Both ultraviolet beams were collimated to optimize the intensity on the targeted terminal. A charge-coupled device camera (ORCA-ER) with on-chip binning was used to capture infrared images (300 × 300 pixels) and Ca^{2+} images (19 × 19 pixels) of the terminal (Supplmentary Fig. 9b, c). The fluorescence in the measuring area with background fluorescence subtraction (off-line) was used to calculate the $[Ca^{2+}]_i$. Images were captured using MetaFluor software and analysed by IgorPro (Wavemetrics). For *in vivo* calibration of Ca^{2+}-indicator signals, we introduced Ca^{2+} indicators with an intracellular K-gluconate pipette solution into the terminal (see Supplementary Materials). For Fura-2 imaging, we used exposure times of 30 ms (in photolysis experiments) and 100 ms (for defined $[Ca^{2+}]$ solution injection experiment) with a 2 Hz capture rate. For Fura-4F and Fura-6F imaging, we used 10 ms exposure times with 2 Hz capture rates before the flash, and 10–30 Hz capture rates after the flash. Ca^{2+} relaxation rates were modulated by the ultraviolet-light-illumination during the ratiometric Ca^{2+}-imaging procedure, which was thus adjusted to maintain stable Ca^{2+} levels (see Supplementary Materials).

Data processing and modelling. Release rates were calculated using the Neher deconvolution program (http://www.mpibpc.mpg.de/groups/neher/software/index.html) with a mEPSC size of 30 pA and a measured waveform[31].

Modelling. We applied different kinetic models to fit the data in our experiments (Fig. 5a, b). The conventional one-Ca^{2+}-sensor kinetic model and the allosteric one-Ca^{2+}-sensor kinetic model were simulated as described[11,12,25] (see Supplementary Fig. 13 legend). In our dual-Ca^{2+}-sensor model, each vesicle in the RRP can be released via three independent pathways: (1) Ca^{2+}-independent fusion in the spontaneous mode, that is, direct exocytosis of vesicles from the RRP with a release rate of γ1. An effectivity factor (C) to account for the change in spontaneous release rate in Syt1 and Syt2-deficient synapses was included. (2) Synchronous Ca^{2+}-evoked fusion mode triggered by full occupancy of the five binding sites of the synchronous release Ca^{2+} sensor[12,25]. (3) Asynchronous Ca^{2+}-evoked release triggered by occupancy of two Ca^{2+}-binding sites of an unidentified Ca^{2+} sensor. The Ca^{2+}-binding states can be defined by X*n*Y*m*(*t*), where X*n* represents the state in which *n* binding sites of the Ca^{2+} sensor for synchronous release have been occupied ($n = 0$–5), and Y*m* the state in which *m* binding sites of the Ca^{2+} sensor of asynchronous release have been occupied ($m = 0$–2). α and β represent the binding and dissociation constants, respectively, of the Ca^{2+} sensor for synchronous release; χ and δ the binding constants for asynchronous release, respectively, b is the cooperativity factor, and *t* is the time[34]. Note that X0Y0(0) = RRP. The kinetics of Ca^{2+}-binding states can be described as (Fig. 5c):

when $0 < n < 5, 0 < m < 2$,

$$\mathrm{d}(\mathrm{X}n\mathrm{Y}m)/\mathrm{dt} = \alpha \times (5 - n + 1) \times \mathrm{X}n - 1\mathrm{Y}m \times [\mathrm{Ca}^{2+}]_i + \beta \times \mathrm{b}^n \times (n + 1) \times \mathrm{X}n + 1\mathrm{Y}m - \alpha \times (5 - n) \times \mathrm{X}n\mathrm{Y}m \times [\mathrm{Ca}^{2+}]_i - \beta \times \mathrm{b}^{n-1} \times n \times \mathrm{X}n\mathrm{Y}m + \chi \times (2 - m + 1) \times \mathrm{X}n\mathrm{Y}m - 1 \times [\mathrm{Ca}^{2+}]_i + \delta \times \mathrm{b}^m \times (m + 1) \times \mathrm{X}n\mathrm{Y}m + 1 - \chi \times (2 - m) \times \mathrm{X}n\mathrm{Y}m \times [\mathrm{Ca}^{2+}]_i - \delta \times \mathrm{b}^{m-1} \times m \times \mathrm{X}n\mathrm{Y}m$$

when $n = 0$, $m = 0$,

$$\mathrm{d}(\mathrm{X0Y0})/\mathrm{dt} = \beta \times \mathrm{X1Y0} - 5 \times \alpha \times \mathrm{X0Y0} \times [\mathrm{Ca}^{2+}]_i + \delta \times \mathrm{X0Y1} - 2 \times \chi \times \mathrm{X0Y0} \times [\mathrm{Ca}^{2+}]_i - \gamma 1 \times \mathrm{X0Y0}$$

when $n = 5$,

$$\mathrm{d}(\mathrm{X}n\mathrm{Y}m)/\mathrm{dt} = \alpha \times (5 - n + 1) \times \mathrm{X}n - 1\mathrm{Y}m \times [\mathrm{Ca}^{2+}]_i + \beta \times \mathrm{b}^n \times (n + 1) \times \mathrm{X}n + 1\mathrm{Y}m - \alpha \times (5 - n) \times \mathrm{X}n\mathrm{Y}m \times [\mathrm{Ca}^{2+}]_i - \beta \times \mathrm{b}^{n-1} \times n \times \mathrm{X}n\mathrm{Y}m + \chi \times (2 - m + 1) \times \mathrm{X}n\mathrm{Y}m - 1 \times [\mathrm{Ca}^{2+}]_i + \delta \times \mathrm{b}^m \times (m + 1) \times \mathrm{X}n\mathrm{Y}m + 1 - \chi \times (2 - m) \times \mathrm{X}n\mathrm{Y}m \times [\mathrm{Ca}^{2+}]_i - \delta \times \mathrm{b}^{m-1} \times m \times \mathrm{X}n\mathrm{Y}m - \gamma 2 \times (\mathrm{X}n\mathrm{Y}m)$$

when $m = 2$

$$\mathrm{d}(\mathrm{X}n\mathrm{Y}m)/\mathrm{dt} = \alpha \times (5 - n + 1) \times \mathrm{X}n - 1\mathrm{Y}m \times [\mathrm{Ca}^{2+}]_i + \beta \times \mathrm{b}^n \times (n + 1) \times \mathrm{X}n + 1\mathrm{Y}m - \alpha \times (5 - n) \times \mathrm{X}n\mathrm{Y}m \times [\mathrm{Ca}^{2+}]_i - \beta \times \mathrm{b}^{n-1} \times n \times \mathrm{X}n\mathrm{Y}m + \chi \times (2 - m + 1) \times \mathrm{X}n\mathrm{Y}m - 1 \times [\mathrm{Ca}^{2+}]_i + \delta \times \mathrm{b}^m \times (m + 1) \times \mathrm{X}n\mathrm{Y}m + 1 - \chi \times (2 - m) \times \mathrm{X}n\mathrm{Y}m \times [\mathrm{Ca}^{2+}]_i - \delta \times \mathrm{b}^{m-1} \times m \times \mathrm{X}n\mathrm{Y}m - \gamma 3 \times (\mathrm{X}n\mathrm{Y}m)$$

The total release within Δ*t*:

$$\mathrm{fuse}(t, \Delta t) = [\gamma 1 \times \mathrm{X0Y0} + \gamma 2 \times (\mathrm{X5Y0} + \mathrm{X5Y1} + \mathrm{X5Y2}) + \gamma 3 \times (\mathrm{X0Y2} + \mathrm{X1Y2} + \mathrm{X2Y2} + \mathrm{X3Y2} + \mathrm{X4Y2} + \mathrm{X5Y2})] \times \Delta t$$

where,

$$\text{spontaneous release} = \gamma 1 \times \mathrm{X0Y0} \times \Delta t$$

$$\text{synchronous release} = \gamma 2 \times (\mathrm{X5Y0} + \mathrm{X5Y1} + \mathrm{X5Y2}) \times \Delta t$$

$$\text{asynchronous release} = \gamma 3 \times (\mathrm{X0Y2} + \mathrm{X1Y2} + \mathrm{X2Y2} + \mathrm{X3Y2} + \mathrm{X4Y2} + \mathrm{X5Y2}) \times \Delta t$$

Miscellaneous. Immunofluorescence labelling and immunoblotting experiments were performed essentially as described[19]. All statistical analyses were performed using Student's *t*-test.